Articles

Molecular Dynamics Simulations of Granular Compaction

Francisco X. Sanchez-Castillo and Jamshed Anwar*

Computational Pharmaceutical Sciences, Department of Pharmacy, King's College London, Franklin-Wilkins Building, 150 Stamford Street, London SE1 9NN, United Kingdom

David M. Heyes†

Department of Chemistry, University of Surrey, Guildford, GU2 7XH, United Kingdom

Received February 13, 2003. Revised Manuscript Received June 19, 2003

We have carried out simulations of the compaction of model granular beds constructed from Lennard-Jones (LJ) particles using nonequilibrium molecular dynamics (MD). The systems simulated comprised a model die containing either a single granule or many granules that were compacted uniaxially by a vertically moving top wall. The simulations while atomistic in nature can also be considered to have a mesoscopic significance in that the primary LJ particles represent coarse-grained units that comprise a realistically sized macroscopic granule. This representation enables plastic deformation of the individual granules as well as fusion between granules to be modeled at a fundamental level. As a granule is compressed, the constituent particles move past each other, giving rise to its deformation. In a multigranular system, at the points of contact between granules, the surface particles on adjacent granules interact with each other and reproduce many of the features of intergranular bonding observed in real systems. The proposed model, although simple, captures the essential physics of the compaction process in a transparent way. It is able to encompass the transition from mainly elastic to plastic deformation, which is instrumental in affecting the quality of real tablets. Using the developed model, we have explored the effects of compression rate on the deformation behavior of the powder column, the microstructure, and the integrity of the formed tablet. The simulations reproduced a number of well-known effects found in tableting. At high compaction speeds and increased extent of final compaction the system manifested a strong elastic response, giving rise to a tendency for the tablets to laminate on decompaction. Slower compaction speeds allowed more time for greater internal rearrangement or plastic deformation and produced a more structurally uniform and stable tablet at the end of the cycle. The simulations also revealed the underlying cause for high-pressure "hot" spots and regions of weak interaction within the tablet where failure can occur. These points or regions invariably corresponded to incoherent interfaces between granule boundaries, and in some instances to interstitial atoms. The mechanical stability of the tablet was found to depend on the effectiveness of the consolidation of the granules, enhanced effectiveness being characterized by more coherent granule boundaries, resulting in a more uniform pressure distribution and stronger granule−granule interactions.

I. Introduction

Compaction, a process in which a granular, agglomerated, or powdery material is consolidated into a single body by a compressive force, is widely employed in the manufacturing industry. In mechanical engineering, compaction is used for forming machine parts from metal powder precursors,[1,2] in energy production for making coal logs and briquettes for burning,[3,4] and in the food sector for the manufacture of cheeses[5] and cereals.[6] In civil engineering the process is used to evaluate sites prior to construction.[7,8] The compaction process is also the key stage in the manufacture of pharmaceutical tablets,[9] our main interest here. Phar-

* To whom correspondence should be addressed. E-mail: jamshed.anwar@kcl.ac.uk.
† E-mail: d.heyes@surrey.ac.uk.

(1) Fujiki, A.; Kojima, H.; Aizawa, T. *Mater. Trans.* **2002**, *43*, 348.
(2) Whittaker, D. *Int. J. Powder Metall.* **1998**, *34*, 53.
(3) Gunnink, B.; Li, W. *Powder Technol.* **2000**, *107*, 273.
(4) Liu, H.; Marrero, T. R. *Powder Technol.* **1997**, *94*, 217.
(5) Carter, R. E. *Rheology of Food, Pharmaceuticals and Biological Materials with General Rheology*; Elsevier Applied Science: Oxford, U.K., 1989.

10.1021/cm030176a CCC: $25.00 © 2003 American Chemical Society
Published on Web 08/02/2003

maceutical tablets are by far the most widely used mode of drug delivery and tend to be complex formulations designed to release the drug at a desired rate in vivo. The raw granules that make up pharmaceutical tablets typically comprise 5−30 μm particles of the active components (the "primary particles") aggregated by a sparse, interconnecting matrix of polymer. For these tablets the compaction procedure must be such that the final tablet withstands handling during any subsequent processing (e.g., film coating) and transport but does not impair the release characteristics of the drug from the tablet.

Tableting of pharmaceuticals is plagued by two major problems: "capping" and "lamination", both of which represent tablet breakup as the punch is withdrawn. The capping phenomenon is specific to tablets with convex top and bottom surfaces and involves the breaking off of the top or "cap" of the tablet. Lamination is more general and involves the breakup of the tablet into a number of layers, usually in the middle of the tablet. These problems can be inherent to a material and/or can arise from excessive compaction speed or an initially nonuniform distribution of the powder within the die.[10−12] The quality and functionality of the compacted material will depend on its chemistry, as the bonding between the various primary particles determines how the microstructure responds. The material can deform plastically, where the primary particles rearrange with respect to each other and/or undergo deformation themselves, or (as is more common) give rise to a viscoelastic response comprising mainly plastic deformation coupled with some elastic recoil. If the material is very strongly bonded and is brittle, it may show brittle fracture. High compaction speeds tend to promote an elastic response, and in this limit fracture is more likely to occur.

While extensive laboratory studies have helped to optimize the compaction conditions, characterize materials, and formulate products with appropriate compaction behavior, the compaction process itself is still poorly understood at a microstructural level. This lack of understanding is due mainly to the facts that the process is rapid (occurring in a fraction of a second) and because in situ monitoring is difficult. The important factors that determine the success of this process, particularly the interplay between the imposed conditions and the chemical composition and original physical state of the powdered material, still require further elucidation. Rather than attempting to probe the compaction process in situ in experiment, an alternative approach is to use computer simulation. Earlier attempts at simulating compaction used finite-element methods, which at first were restricted to the rate-independent limiting case.[13,14] An alternative approach is to use discrete, rigid particles whose deformation behavior can be followed by focusing on the interparticle contact zone during attachment and detachment.[15] This approach is referred to as discrete element modeling (DEM). Further developments have included the combined use of the finite and discrete techniques in a single simulation,[16] where the particles are represented by a finite element mesh and the interactions between the particles and the evolution of the granular bed followed using the DEM approach.

Recently, we used DEM in the form of nonequilibrium molecular dynamics (NEMD) to study compaction[17] and showed that this technique can capture the essential physics of the process. In the molecular dynamics (MD) technique, the trajectories of the interacting particles follow Newtonian dynamics.[18,19] A typical system size in MD simulations is of the order of a thousand particles, which rules out a fully atomistic approach. In the above study the granule was represented by a cluster of about a thousand, soft spherical particles interacting with a Lennard-Jones (LJ) potential. While these particles are formally atoms in a "nano-die", we could also view them as primary particles making up a macroscopic granule. This representation of a granule in terms of multiple subunits is significant since it enables granular plastic deformation to be modeled essentially from first principles. When such a granule is compressed, the constituent particles in the granule move past each other while still remaining part of the same granule, giving rise to the required overall deformation of the granule.

In the present contribution we communicate the results of a more thorough study where we have extended the methodology to a multigranular system. We show that the fusion or bonding between granules, which is an essential aspect of the real process, comes out naturally from the particle−particle interactions in the simulations. When the granules make contact, the particles at the surface interact with those on the surface of another granule in much the same way as particles interacting within a granule, thus modeling the bonding between granules. The proposed model for compaction has the potential to make the compaction process transparent, and hence enable the exploration of the many facets and parameters of the process. Insights gained could prove to be invaluable for developing formulations and technology to yield capping and lamination-free tablets.

(6) Tripodi, M. A.; Puri, V. M.; Manbeck, H. B.; Messing, G. L. *Powder Technol.* **1995**, *85*, 241.
(7) Yong, R.; Warkentin, B. P. *Introduction to Soil Behavior*; The Macmillan Company: New York, 1996.
(8) Berry, P. L.; Reid, D. *An Introduction to Soil Mechanics*; McGraw-Hill Company: London, U.K., 1987.
(9) Lieberman, H. A.; Lachman, L.; Schwartz, J. B. *Pharmaceutical Dosage Forms: Tablets, Vol. 2*, 2nd ed.; Marcel-Dekker: New York, 1990.
(10) Monedero, M. C.; Jimenez-Castellanos, M. R.; Velasco M. V.; Munos-Ruiz, A. *Drug Dev. Ind. Pharm.* **1998**, *24*, 613.
(11) Kim, H.; Venkatesh, G.; Fassihi, R. *Int. J. Pharm.* **1998**, *161*, 149.
(12) Marshall, P. V.; York, P.; Maclaine, J. Q. *Powder Technol.* **1993**, *74*, 171.
(13) Michrafy, A.; Ringenbacher, D.; Tchoreloff, P. *Powder Technol.* **2002**, *127*, 257.
(14) Smith, L. N.; Midha, P. S.; Graham, A. D. *Powder Technol.* **1998**, *79*, 94.
(15) Cundall, P. A.; Hart, R. D. In *Proceedings of the 1st Conference on Discrete Element Methods*, Golden, CO, 1989; Mustoe, G. G., Henriksen, M., Huttelmaier, H.-P., Eds.; pp 1−17.
(16) Gethin, D. T.; Ransing, R. S.; Lewis, R. W.; Dutko, M.; Crook, A. J. L. *Comput. Struct.* **2001**, *79*, 1287.
(17) Sanchez-Castillo, F. X.; Anwar, J.; Heyes, D. M. *J. Chem. Phys.* **2003**, *118*, 4636.
(18) Heyes, D. M. *The Liquid State: Applications of Molecular Simulations*; John Wiley & Sons Ltd: London, U.K., 1998.
(19) Allen, M. P.; Tildesley, D. J. *Computer Simulation of Liquids*; Oxford Science Publications: Oxford, U.K., 1987.

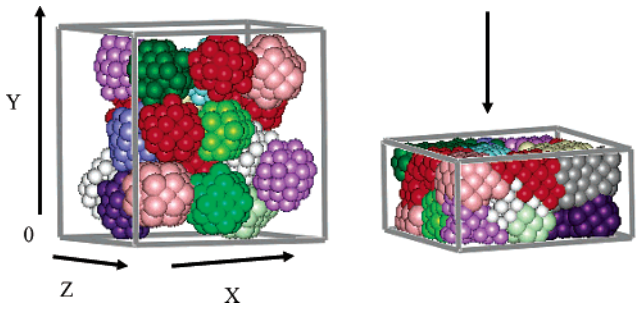

Figure 1. Initial configuration of the multigranular system. This figure shows the granules with a face-centered cubic lattice structure confined within an orthorhombic simulation box. The figure on the left is the initial arrangement of granules before compaction. The figure on the right shows uniaxial compression by the top wall along the *y* direction at a time just before maximum compaction.

II. Method

While the focus of the study is on a multigranular system, we also present some results from the earlier study on the compaction of a single granule[17] for comparative purposes. The single granule consisted of a cluster of 1004 spherical particles while the multigranular system contained 22 spherical granules, each containing between 48 and 52 particles. The initial configuration of the multigranular system is shown in Figure 1. The interaction between the primary particles in each case was through the Lennard-Jones ("12−6") potential combined with a switching function to truncate the potential smoothly to zero at r_{max} starting at r_{min},

$$U(r) = 4\epsilon\left[\left(\frac{\sigma}{r}\right)^{12} - \left(\frac{\sigma}{r}\right)^{6}\right] \qquad \text{for } r < r_{min}$$

$$= 4\epsilon\left[\left(\frac{\sigma}{r}\right)^{12} - \left(\frac{\sigma}{r}\right)^{6}\right]\left[\frac{(r_{max} - r)^2(r_{max} + 2r - 3r_{min})}{(r_{max} - r_{min})^3}\right] \qquad \text{for } r_{min} < r < r_{max} \quad (1)$$

where ϵ and σ set the energy and distance scales of the primary particle−particle interaction and hence the model, respectively. The abrupt truncation of the LJ potential gives rise to a discontinuity in the force at r_{max}, which can in principle give rise to instabilities in the integration of the equations of motion.[20] For the single-granule system the truncation interval was bounded by $r_{min} = 2.3\sigma$ to $r_{max} = 2.5\sigma$. For the multigranular system the truncation interval for the interaction potential was $r_{min} = 1.5\sigma$ and $r_{max} = 1.9\sigma$. The significantly more short-ranged potential for the multigranular system reduced the tendency of the granules to fuse in the early stages of the simulation. This short-ranged potential actually gives the simulations a mesoscopic significance. In real granules where the characteristic microstructural length scale is of the order of micrometers, the intergranule interactions in relative terms are extremely short-ranged. An alternative implementation of a short interaction would be to utilize higher powers in the Lennard-Jones function rather than the 12−6 form. This approach was explored but was found to be both computationally inefficient and not useful; the resulting steeper particle−particle interaction necessitated a significantly shorter time step.

The LJ particles inside each granule were initially arranged on a face-centered cubic (fcc) lattice. The starting configuration of the multigranular system was generated by randomly inserting granules in the model die that was represented by an orthorhombic simulation box (see Figure 1). The walls of the simulation box were perfectly smooth, and the particles interacted with the walls solely as a function of the perpendicular distance from the wall surface, using the Weeks−Chandler−Anderson (WCA) potential form,[21] which is a truncated LJ potential, shifted upward by the well depth ϵ. This potential is purely repulsive, with the potential dropping off to zero at a distance of $2^{1/6}\sigma$ from the wall. We point out that there are no periodic boundaries in the model. The side walls are an important feature of real dies and consequently it was considered essential to include them in the model.

The molecular dynamics simulations were carried out using a program that was developed by Sanchez-Castillo.[22] The program employed Verlet's leapfrog algorithm for integrating the equations of motion. The system was thermostated at each time step using the velocity rescaling method of Woodcock.[23] We discovered that it was necessary to thermostat the system in some way, as the relatively small number of degrees of freedom in the system were not able to accommodate the kinetic energy in plastic deformation, resulting in the melting of the solid. The uncontrolled kinetic energy also gave rise to a substantial, effective "elastic" response even at the lowest compaction speeds. The issue of thermostating in these simulations and its significance with respect to the real process is discussed in a little more detail in our first contribution on this subject.[17] We recognize that out of equilibrium the concept of a temperature is controversial, and there will have been deviations from a Maxwell−Boltzmann distribution. Also, as the average velocity in the *y* direction during the cycle was inhomogeneous throughout the system, a definition of a local reference frame (needed to define the so-called "peculiar" velocities to define a temperature) was difficult to specify uniquely. Initially, we tried thermostating the particles next to the walls but this proved insufficient and so a global damping of the velocities was used. All three components (*x*, *y*, and *z*) of the particle velocities were rescaled equally based on the overall kinetic energy of the system. In this way one does not unduly bias the *y*-component (vertical) of the particle velocities, which is expected to play an important role in the deformation/relaxation processes in real systems. The time step (δt) employed was $0.002\sigma(m/\epsilon)^{1/2}$ for both the single-granule and multigranular systems. The simulation temperature was chosen so that the granules would be in the crystalline part of the LJ phase diagram[24] to prevent vaporization of the primary particles. For the single granule $T = 0.1\ \epsilon/k_B$ and $\rho = 0.9\ \sigma^{-3}$, while for the multigranule systems a lower temperature of $0.05\ \epsilon/k_B$ was employed to restrict the early fusion of the granules simply through thermal diffusion. The simulation temperature was about an order of magnitude smaller than the probable triple-point temperature of this system to ensure that the solid phase was the most stable and to minimize surface melting of the clusters. Time is often referred to as t_{red}, which is the elapsed simulation time as a fraction of the total simulation time. In these reduced units, the time at which maximum compaction occurred is 0.5.

Each simulation comprised a compaction and a decompaction stage. During the compaction stage the top wall moved down at a fixed speed to a point of maximum compaction. This was immediately followed by the decompaction stage in which the displacement direction of the top wall was reversed to enable it to eventually return to its original position. For any given simulation, the speed of the top wall was the same during the compaction and decompaction stages. The single-granule and the multigranule systems were compressed at three compaction speeds, $V = 0.5$, 0.06, and 0.005 $(\epsilon/m)^{1/2}$, so that we could investigate the effects of strain rate. Two series of multigranular simulations were carried out, the difference being the extent of strain of the granular bed at maximum compaction. In Series A the granules were overcompressed,

(20) Nicolas, J. J.; Gubbins, K. E.; Streett, W. B.; Tildesley, D. J. *Mol. Phys.* **1979**, *37*, 1429.

(21) Weeks, J. D.; Chandler, D.; Anderson, H. C. *J. Chem. Phys.* **1971**, *54*, 5237.

(22) Sanchez-Castillo, F. X. *Compaction of Powders by Molecular Dynamics*; Ph.D. Thesis, King's College London, University of London, 2001.

(23) Woodcock, L. V. *Chem. Phys. Lett.* **1971**, *10*, 257.

(24) Agrawal, R.; Kofke, D. A. *Mol. Phys.* **1995**, *85*, 23.

while in Series B the compression was more optimum to minimize the risk of tablet failure during the decompaction stage. For Series A the cross-sectional area of the box in the *xz* plane was 16.4 × 16.4 σ with a *y* direction gap of 3.3 σ at maximum compaction while for B the corresponding values were 15.4 × 15.4 σ and 4.6 σ. The resulting densities of the granule bed at maximum compaction were 1.2 and 0.98 for series A and B, respectively.

We appreciate that the particle−particle interactions could be more sophisticated, as there are no frictional and gravitational forces in the model. We have, however, at this stage endeavored to keep the model simple, to elucidate any features that are in some sense "universal" and independent of length and time scale of the model, rather than due to details of the pair potential.

III. Results and Discussion

Results are presented for various forms of analyses that include structural changes, energetics, and deformational behavior. An important aspect of the analyses presented is that we have adopted some of the classical methods employed in laboratory studies to characterize the deformation behavior of powders during the compaction process. In this respect, the data have been analyzed using force−time plots,[25,26] force−displacement curves,[9,27] compaction profiles,[9] and Heckel plots.[28]

The simulation of the compaction process for the multigranular system is illustrated in a three-dimensional perspective in Figure 1, which shows the initial configuration and another later in the cycle. Note that compaction is in the *y* direction. Snapshots for some representative multigranular systems are given in Figures 2−4 at various stages of the deformation. Projected views of the top and the side of the simulation box are shown in each case.

We focus first on the Series B simulations where the granules were compacted to a density that was relatively lower than those of Series A. The initial impact between the top wall and granules had an effect that differed with wall speed. For the fastest speeds (V = 0.5) it was observed (in Figure 2) that initially only the granules near the top of the box were deformed by the top wall, as a result of the high-velocity impact, while those further below toward the bottom of the die showed no noticeable distortion. For the medium and slowest speeds (see Figure 3), the effects of the first wall engagement were felt more uniformly throughout the box. In these cases the impact-induced distortion of the granules was minimal and all the granules were pushed downward by the top wall in a cooperative fashion. For the fastest speed the granules at the bottom were deformed only near the end of the compaction stage (Figure 2) while at the slower speeds the deformation was more homogeneous, with all granules both at the top and at the bottom being involved in the deformation and reorganization process from an early stage (Figure 3).

The manner in which the granules coalesce must surely be an important issue in governing the quality

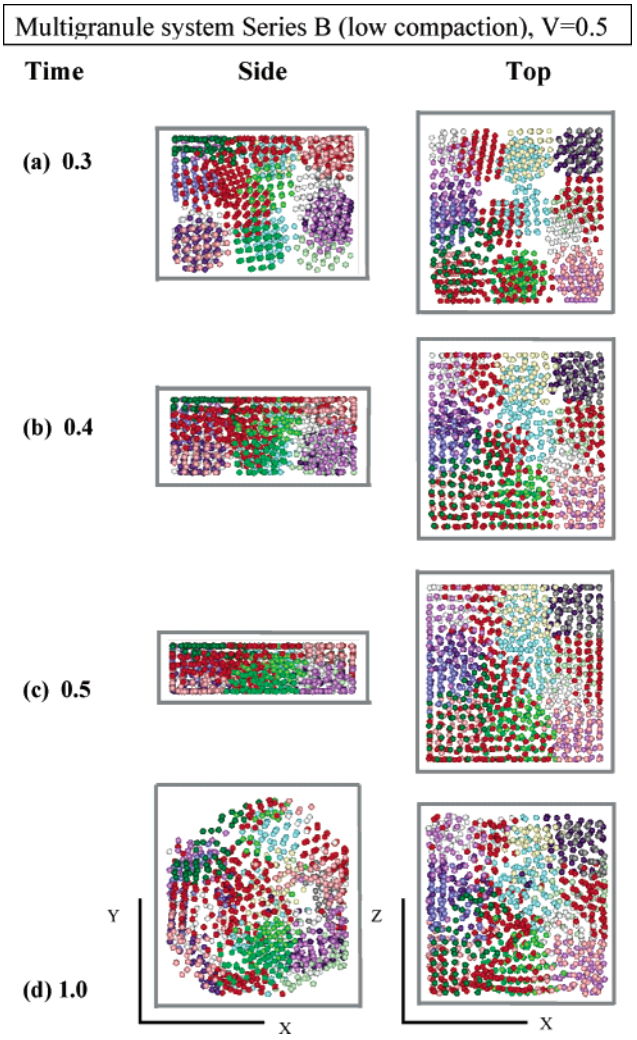

Figure 2. Snapshots of structural changes of the Series B multigranule system (compaction to a low density) during the compaction process for the fastest compaction speed (V = 0.5). Snapshots (a) and (b) are before maximum compaction, (c) at the time of maximum compaction, and (d) at the end of the process after decompaction with the top wall returned to its original position. The time shown on the left side is in units of the total simulation time to complete the compaction and decompaction stages.

of the tablet. It is clear that initially the boundary planes of particles between the different granules were distributed relatively randomly (see Figures 2 and 3). As we will show below, these boundary zones largely coincided with the locations of the high internal pressures at the point of maximum compaction. The initial fcc structure inside the granules broke down in the early stages of the compaction process. At least for the slowest speed of Series B ("optimum compression") it is evident that a relatively homogeneous face-centered-cubic structure was regenerated at maximum compaction and at the end of the compaction process (t_{red} = 0.5 and t_{red} = 1.0, respectively, in Figure 3). In contrast for the fastest speed a more disordered structure was observed at maximum compaction and at the end of the process, as seen in the bottom images of Figure 2. To summarize, the compaction speed had a marked effect on the structure of the final tablet. For the slowest speed, a more or less perfect fcc tablet adopting the shape of the box was formed on withdrawal of the upper wall.

(25) Yliruusi, J. K.; Antikainen, O. K. *Drug Dev. Ind. Pharm*. **1997**, *23*, 69.
(26) Yliruusi, J. K.; Merkku, P.; Hellen, L.; Antikainen, O. K. *Drug Dev. Ind. Pharm*. **1997**, *23*, 63.
(27) Alderborn, G.; Nystrom, C. *Pharmaceutical Powder Compaction Technology*; Marcel Dekker Inc: New York, 1996.
(28) Heckel, R. W. *Trans. Mater. Soc. A.I.M.E.* **1961**, *221*, 671.

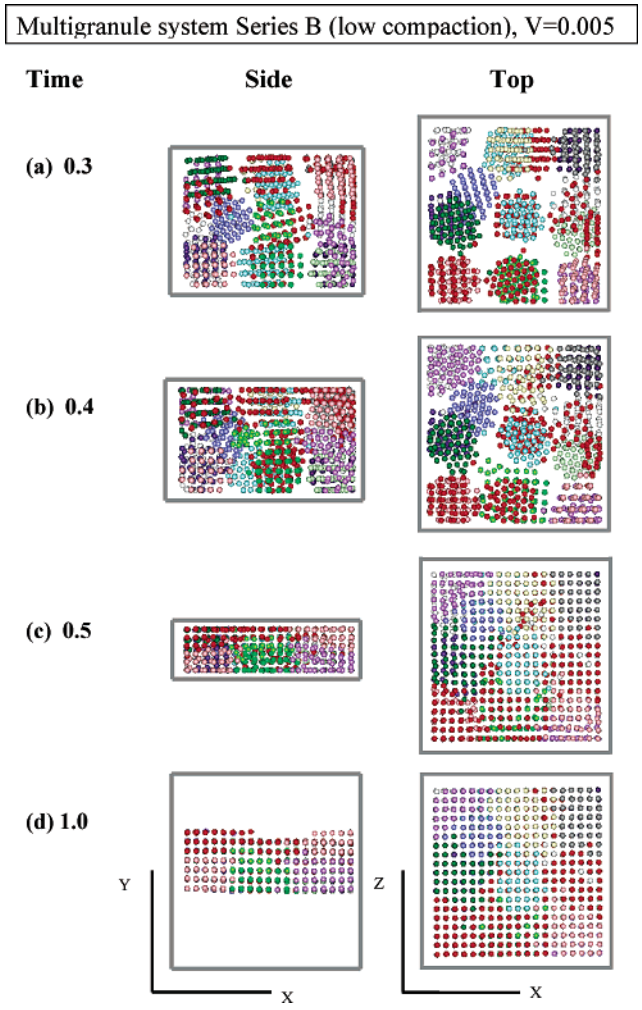

Figure 3. Snapshots of structural changes of the Series B multigranular system during the compaction process for the slowest compaction speed ($V = 0.005$). Snapshots (a) and (b) are before maximum compaction, (c) at the time of maximum compaction, and (d) at the end of the process after decompaction with the top wall returned to its original position. The time shown on the left side is in units of the total simulation time to complete the compaction and decompaction stages.

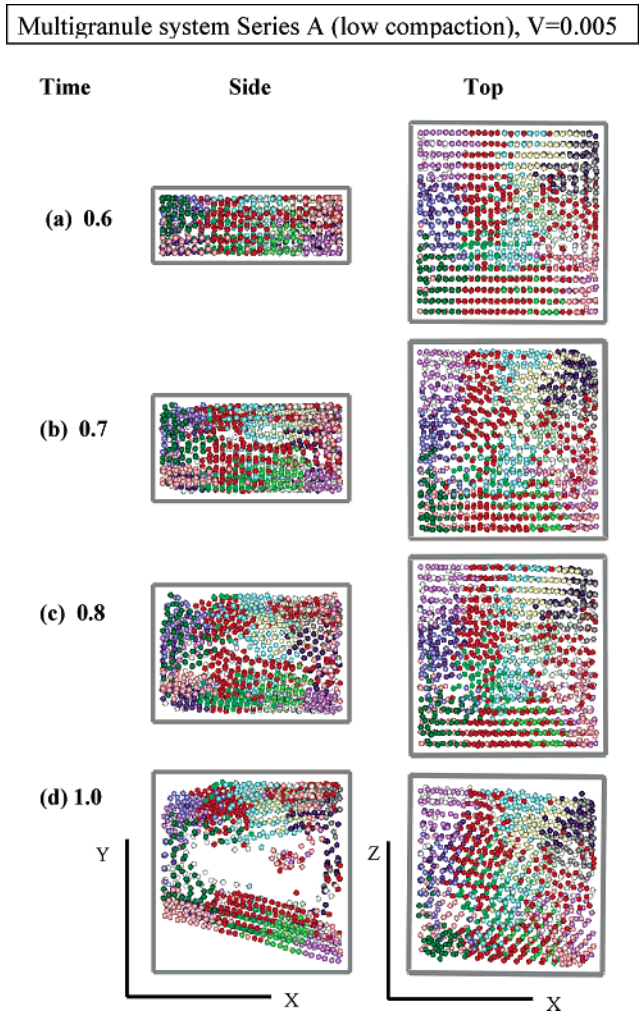

Figure 4. Snapshots of structural changes of the Series A multigranular system (compaction to a high density) during the compaction process for the slowest compaction speed ($V = 0.005$). Only the decompaction stage of the process is shown. The time shown on the left side is in units of the total simulation time.

However, for the fastest speed the granules did not have sufficient time to develop coherent interfaces between their surfaces, and as a result the final material did not retain its integrity and showed failure along the boundaries between the constituent granules.

The corresponding views for Series A multigranule simulation (system compacted to a higher density) during the decompaction phase for the slowest speed ($V = 0.005$) are shown in Figure 4. This series of simulations attempted to explore the effects of the extent of final compaction and the granules were compacted to a higher density relative to the extent of compaction for series B. The high extent of compaction produced immediate lamination of the formed tablet on withdrawal of the top wall, presumably as a result of high internal pressures. This phenomenon is also seen in real pharmaceutical tablets when the material is overcompressed. At the earliest stages of the decompaction, the tablet can be seen to break apart in the middle, mainly toward the right of the side projection (Figure 4c, side view). We show later that these regions are associated with high local pressures and high density in the compressed monolith.

The behavior of a single-granule system had many features in common with the Series A multigranular simulations except that the response was more "elastic" in the single-granule case. For the single granule at the slowest speed, the tablet did not laminate on decompression, probably because the elastic response was not sufficient to overcome the long range of attraction between the primary particles (see the discussion below eq 1 in the Method section). The level of ordering in both cases was similar, although the orientation of the fcc lattice was different. For the single granule a top projection revealed some hcp/rhcp order within a fcc matrix, whereas for the multigranule it was just fcc.

The variation in the configurational or potential energy of the system, expressed as the binding energy per particle, as a function of time for each of the compaction speeds for the single granule and the series B multigranular system is displayed in Figure 5. For the single granule, shown in Figure 5a, initially the system was at equilibrium in the fcc structure and the potential energy was at its most negative value, reflecting this favorable arrangement. With compression the

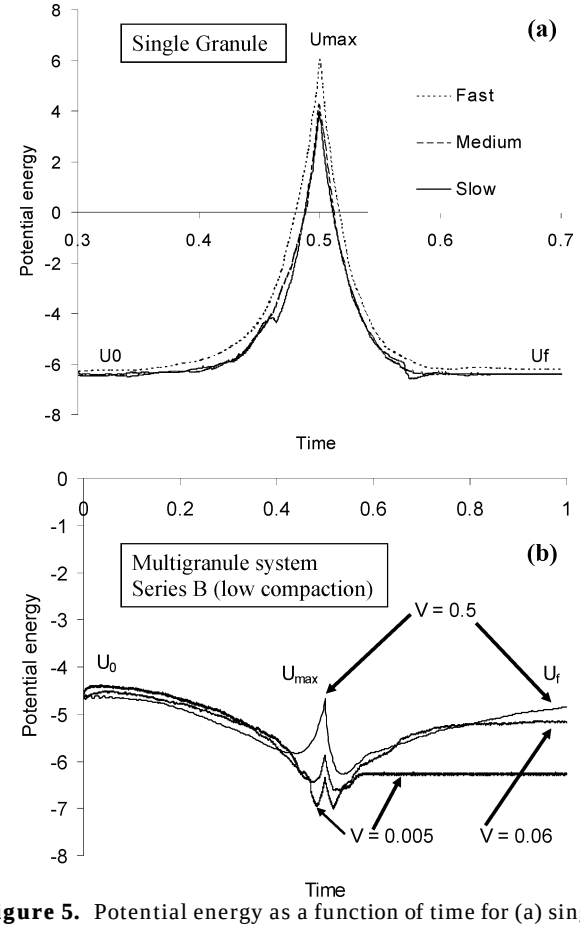

Figure 5. Potential energy as a function of time for (a) single-granule and (b) multigranular system (Series B) for the compaction process. Data for the three compaction speeds, $V = 0.5$, 0.06, and 0.005 are shown on both of the figures. The time axis is in units of the total simulation time.

potential energy increased for all speeds. In each case the maximum potential energy occurred approximately at the end of the compaction stage, presumably because at this point the volume of the system was at its minimum and the particles were in their most compressed states. The discontinuities in the potential energy profiles for the slowest speed we associate with structural transformations that only had time to take place on the time scale of this simulation. For the multigranule system (Figure 5b) the potential energy initially decreased with time. We can assume that this was because of the progressive elimination of the surface energy as the granules were forced together and the interactions between the LJ particles on adjacent granules increased. During this stage the interstitial voidage was being progressively squeezed out. However, near the end of the compaction stage, when the incipient tablet was densely packed, the potential energy increased because the particles were being forced to overlap in the repulsive part of their interaction potential. This increase in potential energy was not as marked as in the single-granule case in which there was less internal free space initially. During the early part of the decompaction stage in both cases, the potential energy decreased as a result of the expansion of the tablet and relaxation of the repulsive contacts. For the two fastest speeds (especially) in the multigranular system it can be seen that the potential energy reached a minimum and then began to increase again. This final

Table 1. Average Potential Energy per Particle at the Beginning (before Compaction but after the Initial Relaxation) U_0 and at the End of the Compaction Process, U_f, for the Three Systems Studied at the Three Compaction Speeds

systems	compaction speed $(\epsilon/m)^{1/2}$	U_0/ϵ	U_f/ϵ	$\Delta U/\epsilon$
single granule	0.5	−6.393	−6.287	0.107
	0.06	−6.519	−6.392	0.127
	0.005	−6.525	−6.385	0.140
series A	0.5	−4.223	−4.687	−0.464
(compaction to high density)	0.06	−4.223	−5.007	−0.783
multigranular system	0.005	−4.223	−4.749	−0.526
series B	0.5	−4.646	−4.852	−0.206
(compaction to low density)	0.06	−4.646	−5.175	−0.528
multigranular system	0.005	−4.646	−6.283	−1.636

Also given is $\Delta U = U_f - U_0$.

stage of increase of energy we attribute to the lamination or breaking up of the tablet in which some near-neighbor "bonds" are broken. For the fastest compaction speed the tablet laminated as seen in Figure 2 for $V = 0.5$, while for the medium-speed case (not shown) the tablet did not laminate but broke up in its lower section, which can be considered as an intermediate between the behavior seen in Figures 2 and 3. For the lowest speed the potential energy versus time plot shows a small minimum after the compaction stage before leveling off to a constant low value. This supports the previous observation, based on the structure, that the final tablet in this case had essentially perfect crystalline order.

The difference in the potential energy at maximum compaction and the initial value is a measure of the elastic energy stored by the system at maximum compaction. This stored elastic energy tends to be lower for slower compaction speeds, as at the slower compaction speeds the particles had greater opportunity to move past each other to find configurations of lower energy. The stored elastic energy is considered to be an important parameter, as it would compete with the cohesive energy of the consolidated material in determining whether the resultant tablet will remain intact or not on punch withdrawal. The average potential energy per particle at the beginning (before compaction but after the initial relaxation) denoted by U_0, and at the end of the compaction process, U_f, is given for the three systems studied at the three compaction speeds in Table 1. These characteristic energies are also indicated on Figure 5. Considering first the single-granule simulation, the two slower speeds had the lowest initial and final energies, presumably because these granules had a greater time to relax before deformation was initiated and a longer time to achieve an optimum arrangement during the cycle. In all cases the energy of the deformed granule at the end of the process was higher than that at the beginning, although in absolute terms these energy changes are really quite small (at the most only a 2% change between the starting and final configurations). Some increase is expected as the starting configuration of the single granule is the stable perfect fcc lattice and any deformation from this will increase the potential energy. In contrast, for the multigranule cases, Series A and B, the final energy is always more negative than the initial energy. The difference $(U_f - U_0)$ became more negative as the compaction speed decreased. This is consistent with there being more plastic deformation for slower compaction speeds to form more stable

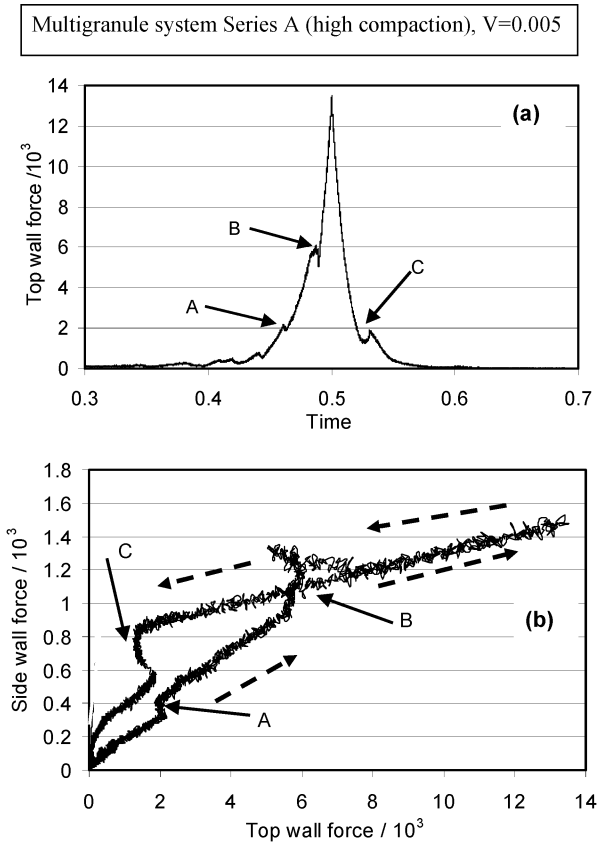

Figure 6. (a) Top wall force as a function of time and (b) top wall force vs side wall force for the multigranular system Series A (high compaction) at the slowest compaction speed ($V = 0.005$). The upward-pointing dashed arrows indicate compaction and the downward-pointing dashed arrows indicate the decompaction stage of the process. Arrows A and B indicate times when there are major ordering structural changes or plastic deformation during compaction, and arrow C indicates an elastic response associated with a disordering transition during decompaction. The letters A, B, and C on both figures (a) and (b) correspond to the same times.

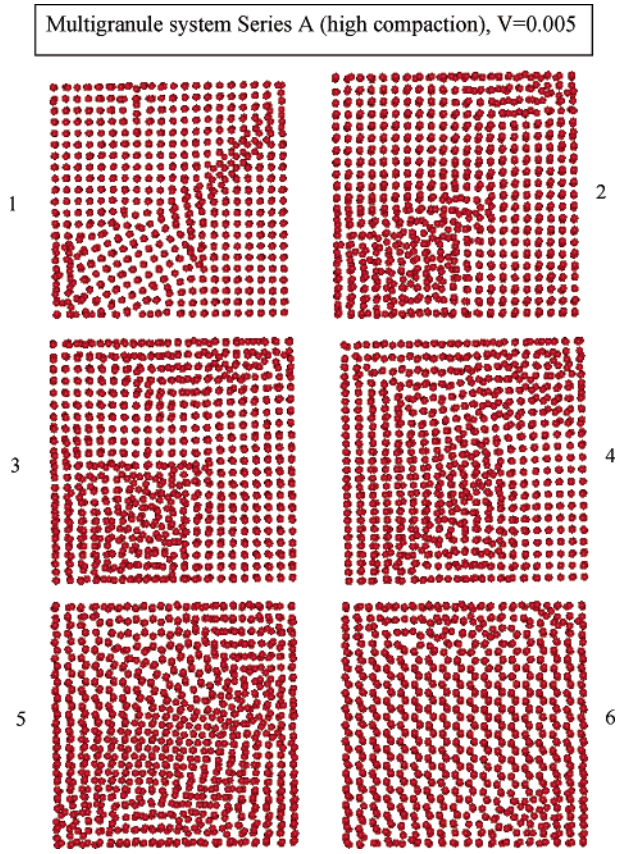

Figure 7. Successive structural changes of the tablet during the plastic deformation just before maximum compaction for the Series A multigranule case at the slowest compaction speed ($V = 0.005$). The view is from the top of the die. The reduced time for each configuration is (1) 0.47, (2) 0.487, (3) 0.488, (4) 0.49, (5) 0.492, and (6) 0.494. The associated wall forces over this time period are given in Figure 6, arrow B.

structures. For Series B there is a more consistent trend in the U_f values in that the slower the compaction speed, the lower the energy of the resulting body. For Series A, this trend is complicated by either the breaking up of the tablet or its lamination on removal of the top wall for the faster compaction speeds. (The intermediate speed showed the greatest energy decrease in this series.)

When significant plastic deformation occurred in the simulations, the primary particles did not simply move past each other into more favorable positions in a uniform way but rather showed one or more abrupt transitions. An extreme case of such a transition occurred with the Series A multigranule system at the slowest speed ($V = 0.005$). The time development of the top wall force and the variation in the side wall force within the die as a function of the top wall force for this system are shown in (a) and (b), respectively, of Figure 6. The latter plot is often referred to as a "compaction profile",[9] a correlation between the lateral or sideways force and the top wall force. The two are coupled because as the vertical stress increases in the uniaxial compaction, the material attempts to expand in the lateral direction, which therefore increases the pressure component in that direction. The hysteresis area within a compaction profile is another indicator of the type of response exhibited by the material, being greater the more plastic the response. The time points indicated by A and B in Figure 6a,b represent periods of significant plastic deformation during which the system transformed in a cooperative way from one highly ordered state to another. At these points there was a large increase in the side wall force for little increase in top wall force. Point C in contrast indicates basically a disordering transition during the decompaction stage while the material was responding elastically. The transition point B can be correlated with a major reorientation of the particle lattice. The time evolution of the microstructure for transition B is shown in Figure 7. Initially, just before the deformation event, the structure shows significant order in the horizontal plane. Most of the structure is coherent but for a small crystallite at the bottom left-hand corner, which has a different orientation, revealing a diagonal boundary plane (Figure 7, frame 1). There is a mismatch at the boundaries between this crystallite and the rest of the structure. As compaction proceeds, the volume becomes further restricted and the possible number of layers of particles that can be accommodated in the vertical direction was reduced from five to four. Thus, the material faces the problem of reconstructing a four-layer structure from a five-layer structure. This transition seems to have been initiated by structural changes

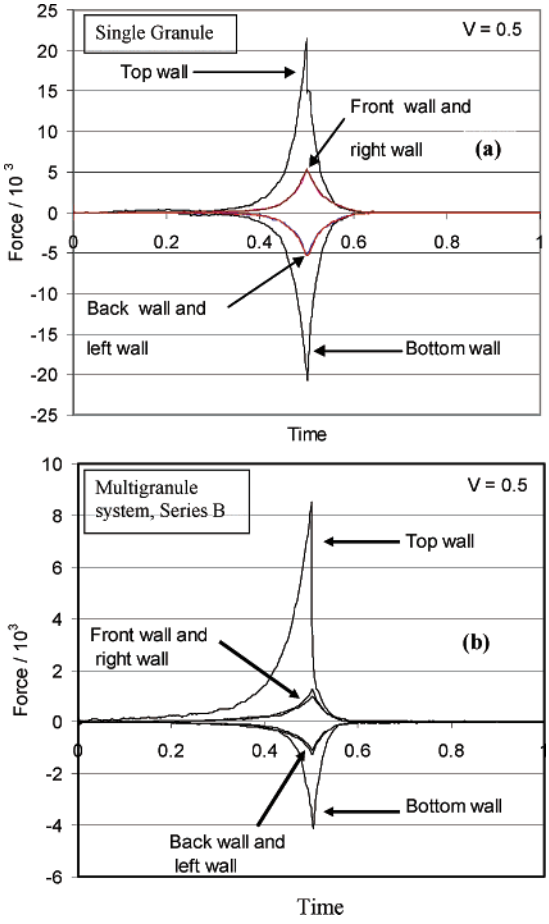

Figure 8. Forces exerted on the walls by (a) single granule and (b) Series B multigranule system as a function of time during the compaction process at the fastest compaction speed ($V = 0.5$). Forces acting downward or to the left or back of the box are represented by negative values to aid discrimination between the different plots.

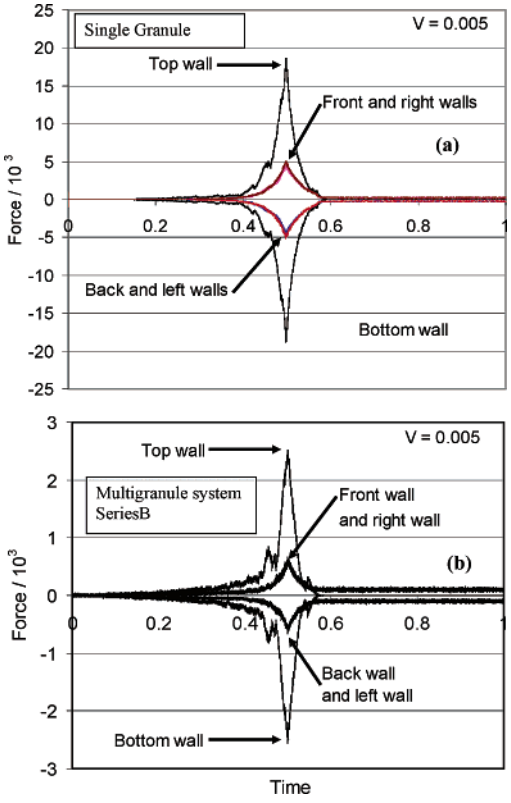

Figure 9. Forces exerted on the walls by (a) single-granule and (b) Series B multigranule system as a function of time during the compaction process at the slowest compaction speed ($V = 0.005$). Forces acting downward or to the left or back of the box are represented by negative values to aid discrimination between the different plots.

resulting in disorder at both the top right-hand corner of the tablet and the bottom left-hand corner corresponding to the site of the small crystallite (frame 2). It can be seen that by frame 6 there has been a reorientation of the lattice structure when compared with frame 1. This "frustrated" final state is we assume the reason the final potential energy of the $V = 0.005$ system was more positive than that of the medium speed $V = 0.06$ system, which did not undergo a similar transformation (see Table 1, fourth and fifth rows of data). (Otherwise, we would expect the lowest speed to have formed the most stable structure and hence the most negative energy.)

The time dependence of the wall forces for (a) single-granule and (b) multigranule Series B simulations for the fastest compaction speed ($V = 0.5$) is shown in Figure 8. The top and bottom wall forces increase with extent of compaction in both cases. The forces in the y direction (vertical axis) are always larger than those in the x and z directions. There is also an asymmetry in the top wall force profiles on either side of the maximum value. The top wall of the box registers a force first as it initiates the compaction. At this fast compaction speed there is inadequate time for the granule or granules to move away from their initial positions and they deform significantly on impact before being displaced downward to interact with the bottom wall (see Figure 2). During the decompaction stage, there is a rapid decay in the top wall force in both cases, which we attribute to the relatively rapid removal of the top wall, and some partial loss of contact of the tablet with it. This effect is more striking for the multigranule case. For comparison, the variation in the wall forces as a function of simulation time for the slowest compaction speed ($V = 0.005$) is shown in Figure 9 for the single-granule and multigranule (Series B) cases. At this speed the profiles are more symmetrical and the level of force transmission between top and bottom walls is better as these systems have a longer time to equilibrate during the cycle. The oscillatory fine structure on the top and bottom wall forces during the compaction stage (particularly for the multigranule case) reflects the structural changes associated with the plastic behavior.

Table 2. Top (F_T) and Bottom (F_B) Wall Forces and the Average Acceleration per Particle for the Series B Multigranule System at the Point of Maximum Compaction for Three Compaction Speeds

compaction speed/$(\epsilon/m)^{1/2}$	$F_T/10^3\ \epsilon\sigma^{-1}$	$F_B/10^3\ \epsilon\sigma^{-1}$	F_B/F_T	acceleration per particle/$\epsilon\sigma^{-1}$ m^{-1}
0.5	8.46	3.41	0.40	4.72
0.06	3.20	3.09	0.97	0.11
0.005	2.48	2.48	1.00	0.00

The maximum force registered by the top and bottom walls, which occurs at the points of maximum compaction, for the Series B multigranule systems at the three compaction speeds is given in Table 2. The average acceleration per particle (a_y) in the direction of movement of the top wall can be calculated using Newton's

second law, $a_y = \Delta F_y/m$, where m is the mass of the entrained material and ΔF_y is the net force on the assembly in the vertical direction. The calculated accelerations are also given in Table 2. The acceleration values indicate that the systems with the medium and slowest speeds are evolving slowly with negligible acceleration and thus can be treated as being quasi-static systems at all times. The extent of transmission of the top wall force to the bottom wall, expressed as the ratio, F_B/F_T, is also given in Table 2 for the three compaction speeds. This ratio is a useful parameter employed in the evaluation of solid lubricants employed in compaction.[29] A ratio tending to unity indicates good lubrication of the side walls. In the present simulations there are no frictional forces on the side walls and we would expect this ratio to equal unity, at least in the "quasi-static" limit, with there being essentially full transmission of the top wall force to the bottom wall at each instant. However, for the fastest compaction speed, $V = 0.5$, the transmission is only about 40% (and 93% for the single-granule case). The transmission of force through the layers of particles of the tablet requires a finite time and therefore in this case the granule system is accelerating with a non-negligible value. In contrast, for the two slowest speeds, the extent of force transmission is essentially complete at each instant. For the fastest compaction speed ($V = 0.5$), the maximum bottom wall force in both the single- and multigranule cases occurred slightly after the time of maximum compaction. This time-lag effect we think is due to the consolidated solid acquiring a large momentum downward. For a short time, even after the beginning of the decompaction stage, the momentum gained by the consolidated mass continued to have an effect on the lower layers of the particles. This resulted in a continuous increase in transmitted force on the bottom wall, even though the top wall was moving away by this time. A further consequence was a temporary loss of interaction between the upper surface of the tablet and the receding top wall, manifesting in the sharp drop in the upper wall force at the beginning of the decompaction stage, as can be observed in Figure 8.

The fractional area of contact of the particles with the walls, defined as the projected area of those particles that are within the range of interaction of the wall potential divided by the total area of the wall, is shown for the multigranule Series B as a function of time in Figure 10. For the fastest speed, $V = 0.5$, shown in Figure 10a, it can be seen that it is the top wall that has initially the most contact with the entrained material. The bottom wall contact area is much lower during both the compaction and decompaction stages. For the slowest speed, $V = 0.005$, shown in Figure 10b, the top and bottom wall contact areas are much the same at all times, as we would expect in the quasi-static limit. For both speeds, the extent of contact with the side walls is greater than the top and bottom walls during the later stages of the process. The side wall forces and extent of contact of the tablet with the side walls are important factors in tablet manufacture. They govern the magnitude of force required to eject the tablet from the die and also the amount of lubricant needed on the walls of the die to facilitate this process.

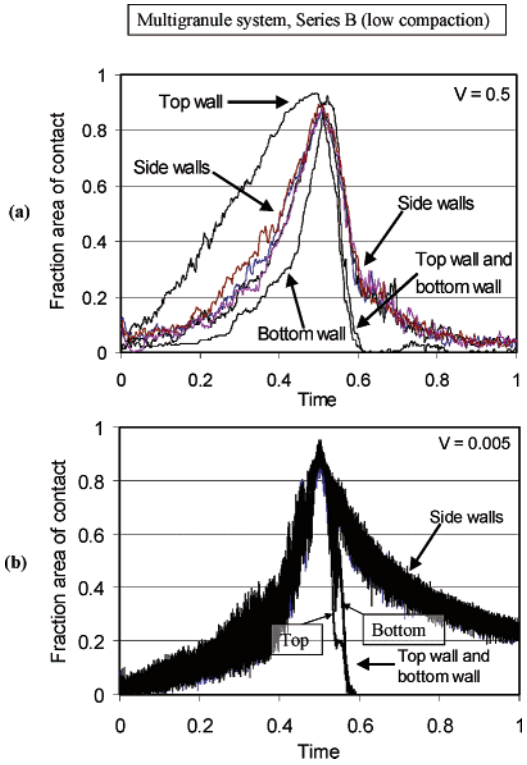

Figure 10. Fractional contact area on the various walls of the simulation box for the Series B multigranule system as a function of time for (a) fastest and (b) slowest compaction speed.

In the laboratory, the force−time curves are often analyzed in terms of their symmetry and partial areas to infer information about the deformational behavior of the material and the mechanism of consolidation.[25,26] The area under the curve is typically subdivided into two sections, from the origin to the maximum compression force, A_C, and from the maximum compression force to the end of the decompaction stage, A_D. The ratio of A_D and A_C is a measure of the curve "symmetry". An ideal elastic material will produce a symmetrical curve and the ratio of its areas will be unity, while for an ideally plastic material A_D would be zero, resulting in an A_D/A_C of zero. For the single granule, $A_D/A_C = 0.49$, 0.71, and 0.68 for $V = 0.5$, 0.06, and 0.005, respectively. For the Series B multigranule systems these ratios are 0.11, 0.45, and 0.45, indicating a more general level of plastic response in the multigranule case. We believe that the relative elasticity (the ratio A_D/A_C) is grossly underestimated for the faster compaction speed because of a reduction in the degree of interaction between the top wall and the granule as the top wall starts to move away from the bottom wall. In fact, because of the significant downward momentum of the compact, the material probably continued to consolidate even while the top wall moved upward. Therefore, not all of the elastic recovery was registered by the top wall. This highlights the potential perils of using force−time plots to derive the true level of elastic vs plastic response of the entrained material.

The work done in compacting the material is considered to be an important parameter for characterizing materials. In laboratory studies this is obtained from a

(29) Lachman, L.; Lieberman, H. A.; Kanig, J. L. *The Theory and Practice of Industrial Pharmacy*, 3rd ed.; Lea & Febiger: Philadelphia, PA, 1986.

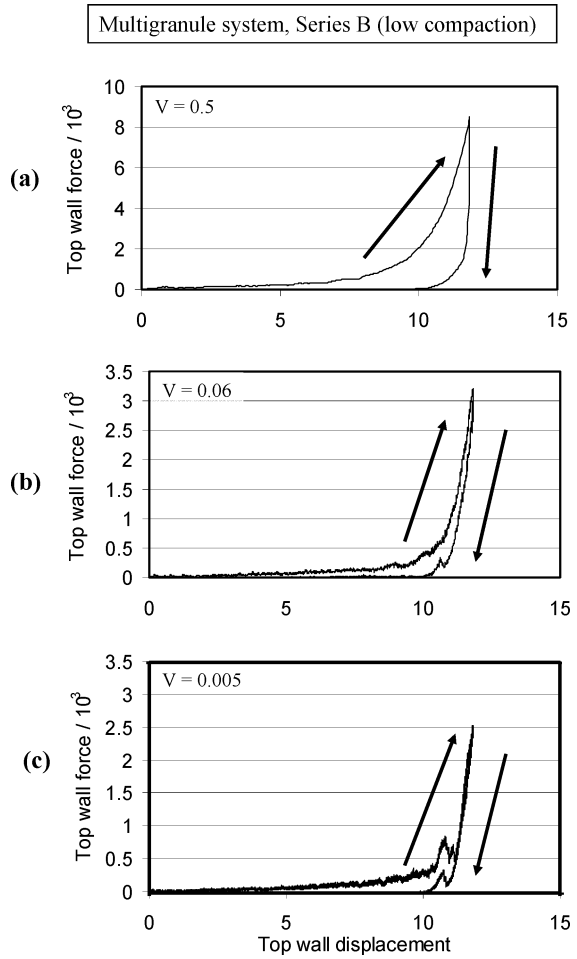

Figure 11. Top wall force for the Series B multigranule system as a function of top wall displacement during the compaction process at the three compaction speeds (a) $V = 0.5$, (b) $V = 0.06$, and (c) $V = 0.005$. The upward-pointing arrows indicate compaction and the downward pointing arrows indicate the decompaction stage of the process.

force−displacement curve where the top wall force is plotted as a function of the top wall displacement.[9,27] The work done is given by the difference in the areas under the curves for the compaction and decompaction stages, A_C and A_D, respectively, as for the force−time curves (with time replaced by distance). The force displacement plots for the multigranule system Series B are given in Figure 11. With increasing speed the system is expected to respond more elastically. Consequently, the hysteresis area (the enclosed area in these figures) should be lower for the higher speeds. However, consistent with the force−time data and for the same reasons as discussed earlier, we observe the opposite.

The densification of the powder column as a function of the applied pressure or stress can be measured through the function proposed by Heckel.[28] If one assumes that the compressibility of the material is proportional to the current porosity, then we arrive at the Heckel equation,[30−32]

$$\ln\left(\frac{1}{1-\frac{D_A}{D_T}}\right) = KP + A \qquad (2)$$

where D_A is the apparent density, D_T is the maximum

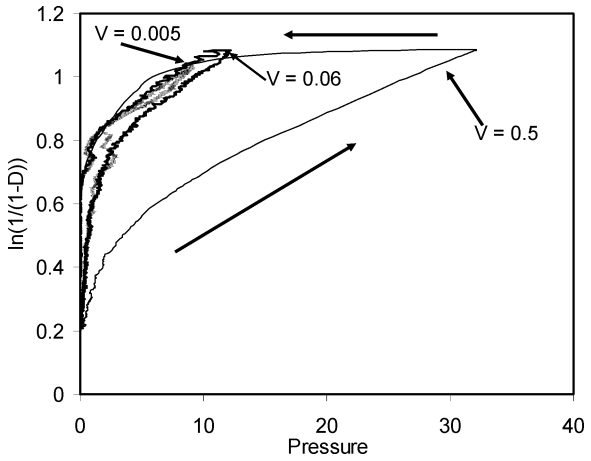

Figure 12. Variation in porosity of the powder column as a function of pressure as defined by the Heckel function (eq 2) for Series B (low compaction) multigranular systems at the three compaction speeds. The upward-pointing arrows indicate compaction and the downward pointing arrows indicate the decompaction stage of the process. D is D_A/D_T as defined in eq 2.

density that can be achieved at high pressure (taken here to be that of the fcc crystal, which is 1.414 in reduced units), K is the slope of the linear portion of the curve, P is the axial pressure, and A is the intercept on the ordinate extrapolated from the linear portion of the curve. The constant A is a measure of the filling density of the particles before appreciable interparticle bonding occurs, while the slope K is the compliance of the material to plastic deformation[33,34] (the yield strength is $1/3K$[28,33]). The term on the left of eq 2 we call the logarithmic densification factor, LDF.

A typical Heckel plot should show some initial curvature (registering the relatively facile initial process of re-packing of the granules) and then an essentially linear response. The Heckel plots for the Series B multigranular systems are shown in Figure 12. The plots are sensitive to compaction speed, even though the LDF (1.08) for the three systems is roughly the same at the highest pressures reached in each case. This difference in form with compaction speed can be attributed to the effect of deformation and distribution of granules inside the die. The initial stage of the profile up to $P \approx 4$, just before the near-linear part, corresponds to the early stages of compaction and the filling in of the interstitial voids. Only for the fastest speed is there a clear linear relationship between the logarithmic densification factor and pressure after the initial compaction stage, and this system requires almost 3 times more pressure than the other systems to reach the same densification. This is probably due to the resistance from the granules, which at $V = 0.5$ had insufficient time to re-organize and yield as might a body with a coherent microstructure. These granules were unable to fuse compatibly to form a homogeneous structure and remained as a number of microcrystallites that had to be forced together. For the two slowest speeds the plastic deformation suffered by these systems enabled them to

(30) Fell, J. T. *Labo-Pharma-Probl. Tech.* **1983**, *31*, 353.
(31) Duberg, M.; Nystrom, C. *Powder Technol.* **1986**, *46*, 67.
(32) Sonnergaard, J. M. *Euro. J. Pharm. Sci.* **2000**, *11*, 307.
(33) Sun, C.; Grant, D. J. W. *Int. J. Pharm.* **2001**, *215*, 221.
(34) Panelli, R.; Filho, F. A. *Powder Technol.* **2001**, *114*, 255.

Table 3. Heckel Parameters Obtained from Fitting Eq 2 to the Simulation Data Shown in Figure 12[a]

compaction speed/$(\epsilon/m)^{1/2}$	A	D_A/D_T	$K/\sigma^3\epsilon^{-1}$	yield strength/$\epsilon\sigma^{-3}$
0.5	0.520	0.41	0.0181	18.5
0.06	0.727	0.52	0.0291	11.5
0.005	0.757	0.53	0.0293	11.0

[a] D_A/D_T (= 1 − exp(−A)) is the ratio of the bulk density of the system to the close-packed value, obtained from the Heckel plot intercept parameter, A, that is, when $P = 0$. The yield strength is $(3K)^{-1}$. The maximum value of the LDF was 1.08 in Figure 12, which corresponds to $D_A/D_T = 0.66$ or $D_A = 0.93$.

achieve the same densification as the fastest speed but at lower pressures. Table 3 gives the parameters defined in eq 2 obtained by fitting to the densification profiles. These parameters show that as the compaction speed decreased, the system could achieve a more compact state of the initial granules (prior to the linear region of the Heckel plot). The compliance of the system also increased with decreasing compaction speed, as these systems were more able to undergo plastic deformation under the later stages of the compression phase.

The "granule strain", γ, defined here as the ratio of the change in the vertical (y) dimension of the granule to its original dimension, for the multigranule Series B at the slowest compaction speed is shown in Figure 13. The vertical dimension was taken to be the distance between the top-most and the bottom-most particles in the system. During the compaction stage there is (in general terms) a constant rate of increase in the strain. At the beginning of the decompaction stage there is an elastic recovery of the tablet (and some slower plastic deformation for the fastest compaction speed). Finally, at the end of the process, for the slowest compaction speed the tablet showed some residual strain as a result of the plastic deformation suffered in the process. For the higher compaction speeds the residual strain (not shown) was effectively zero as the compacts laminated on decompaction.

In experimental analysis the pressure and the density distribution within the tablet are recognized as being important information to obtain as they can identify possible failure zones within the tablet. The pressure on an individual particle has no rigorous statistical mechanical definition. Nevertheless, it was estimated using a formula proposed by Kustanovich et al.[35,36] based on the average pair "force" exerted over the surface of the particle, and normalized by the surface area of a sphere of radius $\sigma/2$ to give the local effective pressure at the position of the particle, P_i^{eff}, that is,

$$P_i^{\text{eff}} = \frac{-\sum_{j \neq i} U'(R_{ij})}{4\pi\left(\frac{o}{2}\right)^2} \qquad (3)$$

where $U' \equiv dU/dR$ and U is the pair potential of eq 1. At the point of maximum compaction the entrained volume in the die was divided into sub-boxes of equal volume on a grid of 12 × 12 × 4 in the x, z, and y directions, respectively, for the single granule. For the multigranule case, the equivalent grid was 16 × 16 × 3 for Series A ("overcompressed" case) and 15 × 15 × 4 for Series B ("low compression"). The pressure within each element of the grid was calculated by averaging the effective pressure, P_i^{eff} from eq 3, for each particle contained within it. The pressure distributions were determined by carrying out separate simulations in which the top wall was kept at the state of maximum compaction for an extended period of time (10% of the usual compaction cycle time), to improve the statistical sampling of the pressure. We focus here on the Series A multigranule system that had been compacted to a nonoptimum, too high a density. For this system, the probability distribution of pressures was Gaussian-like (possibly because of the highly disrupted state produced) for the highest compaction speed but it was bimodal for the slowest speed, reflecting the more extended structures formed. The pressure distribution within the compressed tablet is shown in terms of contour maps for two layers of the tablet for the slowest compaction speed in Figure 14. The tablet is resolved into four layers in the vertical y direction. The contours show that the pressure distribution in the tablet is highly nonuniform, with low-pressure regions tending to be in the top and bottom layers and the highest pressure typically in the middle. Many of the high-pressure regions were coincident with the boundaries between granules as explained below.

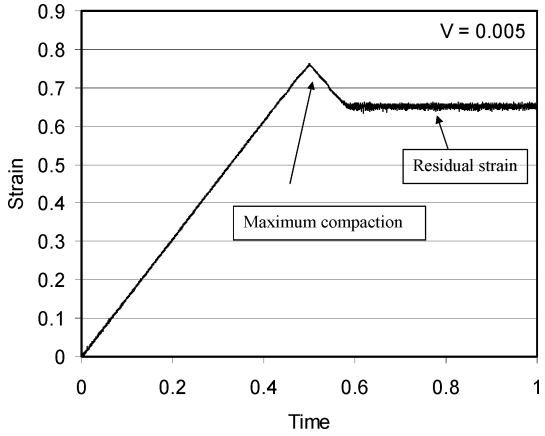

Figure 13. The strain, defined as the ratio of the change in the vertical (y) dimension of the granule to its original dimension, of the Series B multigranule system as a function of simulation time at the slowest compaction speed, $V = 0.005$. Time is in units of the total simulation time.

Tablet failure is thought to occur at regions where the pressures are high and where the elastic recovery overwhelms the binding forces. Little is known about what causes the high-pressure hot spots that give rise to the elastic recoil. The present simulations give some insight into what might be involved. Close inspection of the evolution of the microstructure reveals that the cause for both the high-pressure hot spots and the regions of weak interaction are the mismatched boundaries between the granules where the surface planes are forced together to form a single structure. The high pressures also result from "trapped" particles within these boundary zones. These observations are best illustrated by the more extreme compaction states produced by the multigranule Series A simulations,

(35) Kustanovich, T.; Alexander, S.; Olami, Z. *Physica A* **1999**, *266*, 434.
(36) Kustanovich, T.; Olami, Z. *Phys. Rev. B* **2000**, *61*, 4813.

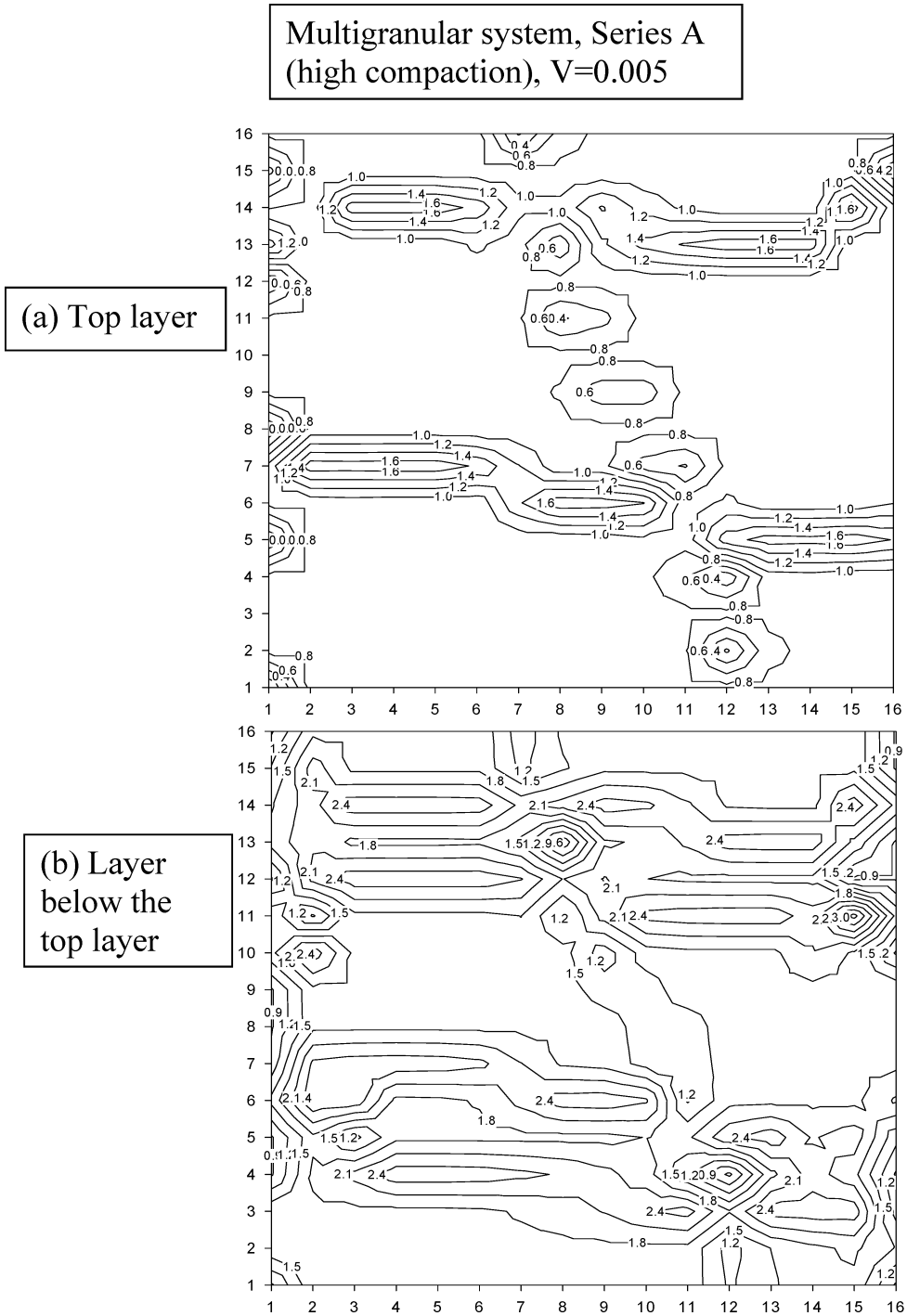

Figure 14. Pressure contours for (a) the top layer and (b) the second from the top layer of the Series A multigranule system (compaction to a high density), averaged over the dwell time at maximum compaction for the slowest compaction speed, $V = 0.005$.

where the granules have been compacted to the highest density. Views from the top and bottom of the simulation cell at maximum compaction for the Series A system at the fastest compaction speed ($V = 0.5$) are shown in Figure 15. This system exhibited the greatest elastic response. The particles of the various granules are shaded differently and on these figures we also show the location of the high-pressure points (averaged over a period of the extra 10% dwell time at maximum compaction). The limitation of the two-dimensional figures is that we can only define the lateral locations and not the depth. On the figure the high-pressure points are marked by squares. Marked squares that are shown "crossed" in the top view in Figure 15 (as specified for example by the letters A and B) indicate high-pressure points that all lie along the boundaries between granules. The letter C specifies other high-pressure "hot spots" that do not appear to be at the boundaries between granules. However, if one views the tablet from another direction, one invariably finds that these are also located along the boundaries between other granules. Thus, in the bottom view, the high-pressure areas specified by C are found to lie at the granule boundaries. There are also other points shown in the top view, specified by "uncrossed" boxes that do not appear to lie at the grain boundaries, but on

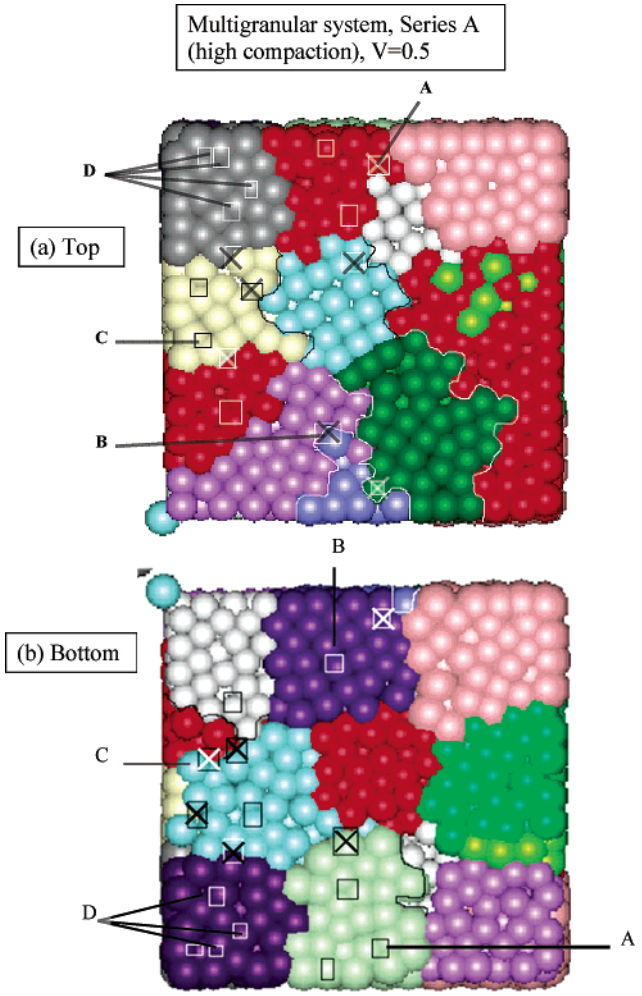

Figure 15. (a) Top and (b) bottom view of the tablet at maximum compaction for the Series A multigranule system at the fastest compaction speed ($V = 0.5$). Space-filling representations of the particles are shown. Particles from the various granules have different shading (colors). Each small square indicates the location of a high-pressure point in the tablet. The crossed squares are those that coincide with the boundaries between the granules. Letters A and B correspond to high pressures in the boundaries between granules at the top surface of the tablet, letter C corresponds to an interface at the bottom surface, and letter D shows the lateral locations of the high-pressure points that can be correlated with interfaces within the tablets. The origin of the simulation cell is depicted by a large fictitious particle that appears in (a) on the bottom left corner and in (b) on the top left corner.

examination of the internal structure of the consolidated mass can also be seen to lie on the internal interfaces or "grain boundaries" within the tablet. The slowest compaction speed also yielded a similar picture. For the latter, there were some regions where the hot spots did not coincide with boundaries between granules. In these locations an interstitial particle was responsible for the large local pressure.

Figure 15 brings into sharp focus the importance of effective fusion of the granules along their boundaries to achieve an incipient tablet that will not break up during the decompaction stage. We have shown that the interface boundaries are where high pressures are likely to develop during the process and therefore most likely to be the points of failure on decompaction. If there is a mismatch between the boundary planes of particles on adjacent granules, this will lead to a weak region in the tablet. This creates a highly disordered structure in the boundary regions that under compaction generates high energies and pressures. Caro et al.[37] discussed this issue and found that the higher the contact angle between two planes of boundary particles, the higher the internal energy and the greater the structural instability.

So far, we have made no recourse to the mesoscopic perspective. The simulations are formally atomistic in scale (as we used LJ particles and Newton's equations of motion) corresponding to compaction of clusters of atoms in a nanodie. In this context we have shown that the time-dependent viscoelastic behavior previously observed at the macroscopic level can also be produced at the atomistic level, so there is significant scale invariance in the response. Further, the causes of failure of the compacted tablet are the incoherent boundaries between the granules and interstitial atoms that can give rise to high-pressure spots. While these results would be invaluable for nanotechnology, a key objective of the present study was to develop a mesoscopic perspective where the LJ particles are viewed as mesoscopic units that comprise a realistically sized macroscopic granule. This raises the issue of how to map the current simulations onto a real system and some discussion of this was given by us in the previous publication.[17] We impose the length scale by defining the size of the granules to be typical of the diameter of pharmaceutical granules, namely, 500 μm. This fixes the size of the individual subparticles (the LJ particles), yielding the real length-scale parameter $\sigma_r \approx 50$ μm. Taking the density of the bulk granules to be 1000 kg m^{-3}, which is the midrange value for pharmaceutical granules, this sets the mass of the individual particles to be $m_r \approx 10^{-11}$ kg. The real-scale interaction well-depth parameter ϵ_r can be obtained from the tensile strength of a powder bed of the material of interest.[17] Using the data for lactose powder,[38] a common excipient of pharmaceutical tablets, we have $\epsilon_r \approx 10^{-13}$ J for ca. 50-μm diameter particles. The equivalent real values of σ_r, ϵ_r, and m_r indicate that the simulation compaction rates need to be multiplied by ca. 0.1 to convert them to m s^{-1}. Typical compaction speeds in pharmaceutical tableting are about 0.2 m s^{-1}, so the simulation compaction speeds (equivalent to 0.0005−0.05 m s^{-1}) are not too far from the real world. To get even closer to the real-world compaction speeds, we see two possible options: (i) to increase the compaction velocity further and/or (ii) to increase the resolution of the granules (i.e., increase the number of primary particles representing each granule). Increasing the compaction velocity will result in a significant amount of the work performed by the top wall being converted into heat that is extracted by the thermostat. This dissipated energy is no longer available to the particles to reorganize into an optimum structure. Increasing the compaction velocity is therefore not a good option. The preferred approach would be to increase the resolution of the granules (i.e., by increasing the number of LJ particles in the system). As the granule resolution increases, the primary particle diameter decreases (keeping the same

(37) Caro, A.; van Swygenhoven, H.; Farkas, D. *Phys. Rev. B* **2000**, *62*, 831.
(38) Schweiger, A.; Zimmermann, I. *Powder Technol.* **1999**, *101*, 7.

granule dimensions in real units). The corresponding equivalent real time scale of the simulation decreases (as σ_r^2 assuming the mass of the primary particle is proportional to σ_r^3). Since the real length scale has also decreased, the effective compaction velocity therefore increases as σ_r/σ_r^2 or $1/\sigma_r$ in real units, that is, the real compaction velocity is inversely proportional to the size of the primary particle.

IV. Conclusions

A key objective of the study was to extend the nonequilibrium molecular dynamics (NEMD) approach developed earlier to simulate the compaction of a single granule to the compaction of a multiple-granule powder bed, which is more typical of real systems. We have shown that this NEMD approach utilizing Lennard-Jones particles (which may also be perceived as spherical elements if the perspective is mesocopic) is able to reproduce the essential physics of compaction of a multigranule system. For the multigranule powder bed not only must the individual granules be able to deform but also the granules must be able to fuse together when the powder bed is compressed. In real materials both the deformation (or fracture) of the individual granules and their fusion are to first order determined by the interactions between the atoms or molecules of the material. Consequently, in the present study we have followed this lead from real systems and have employed the same interaction potential for intragranular and intergranular interactions. This approach plus the requirement that the interaction potential be short ranged (to mimic the very short-ranged intergranular interactions between real granules) has been shown to be effective. Furthermore, simulations at different compaction speeds and different extents of compaction show that the model exhibits essentially all the important features of real systems including strain rate-dependent viscolastic behavior. We attribute the success to the van der Waals type (Lennard Jones) particle−particle interaction employed that is largely responsible for the deformational behavior of real materials. Furthermore, the model reproduces many of the aspects of the observed responses in the real tableting process, such as tablet lamination. If the material is compressed too rapidly, the "recoil" of the entrained tablet can easily result in failure of the tablet on withdrawal of the press, which we have identified as being largely due to pressure "hot spots" along the boundaries between the fused granules. While the time and distance scales of the current model are an order or two magnitudes smaller than those typical of real systems, the fact that the simulations still capture many of the features found in experiments indicates a certain length- and time-scale invariance of such behavior. With ever-increasing computer resources becoming available, future simulations should be carried out with many more primary particles in the system than considered here. The compaction rates of the model and experimental systems will then be closer. It would also enable us to sample a more diverse range of initial conditions for the bed.

Acknowledgment. Francisco Sanchez-Castillo is grateful to the National Council of Science and Technology of Mexico (CONACYT) for the provision of a research studentship under Grant No. 115987.

CM030176A